



The BIG'95 Submarine Landslide—Generated Tsunami: A Numerical Simulation

Author(s): Olaia Iglesias, Galderic Lastras, Miquel Canals, Maitane Olabarrieta, Mauricio González, Íñigo Aniel-Quiroga, Luis Otero, Ruth Durán, David Amblas, José L. Casamor, Elias Tahchi, Stefano Tinti, Ben De Mol

Reviewed work(s):

Source: *The Journal of Geology*, Vol. 120, No. 1 (January 2012), pp. 31-48

Published by: [The University of Chicago Press](http://www.press.uchicago.edu)

Stable URL: <http://www.jstor.org/stable/10.1086/662718>

Accessed: 03/05/2012 04:51

Your use of the JSTOR archive indicates your acceptance of the Terms & Conditions of Use, available at <http://www.jstor.org/page/info/about/policies/terms.jsp>

JSTOR is a not-for-profit service that helps scholars, researchers, and students discover, use, and build upon a wide range of content in a trusted digital archive. We use information technology and tools to increase productivity and facilitate new forms of scholarship. For more information about JSTOR, please contact support@jstor.org.



The University of Chicago Press is collaborating with JSTOR to digitize, preserve and extend access to *The Journal of Geology*.

The BIG'95 Submarine Landslide–Generated Tsunami: A Numerical Simulation

Olaia Iglesias,¹ Galderic Lastras,^{1,} Miquel Canals,¹ Maitane Olabarrieta,²
Mauricio González,² Íñigo Aniel-Quiroga,² Luis Otero,³ Ruth Durán,¹ David Amblas,¹
José L. Casamor,¹ Elias Tahchi,¹ Stefano Tinti,⁴ and Ben De Mol¹*

*1. Grup de Recerca Consolidat Geociències Marines, Universitat de Barcelona, E-08028 Barcelona, Spain;
2. Instituto de Hidráulica Ambiental, Universidad de Cantabria, E-39005 Santander, Spain; 3. Departamento
de Física, Universidad del Norte, Barranquilla, Colombia; 4. Dipartimento di Fisica, Settore di Geofisica,
Università di Bologna, 40127 Bologna, Italy*

ABSTRACT

This article presents a reasonable present-day, sea-level highstand numerical simulation and scenario for a potential tsunami generated by a landslide with the characteristics of the BIG'95 debris flow, which occurred on the Ebro margin in the western Mediterranean Sea in prehistoric times (11,500 cal yr BP). The submarine landslide deposit covers an area of 2200 km² of the slope and base of slope (200–1800-m water depth), involving a volume of 26 km³. A leapfrog finite difference model, COMCOT (Cornell multigrid coupled tsunami model), is used to simulate the propagation of the debris-flow-generated tsunami and its associated impact on the nearby Balearic Islands and Iberian coastlines. As a requisite of the model, reconstruction of the bathymetry before the landslide occurrence and seafloor variation during landsliding have been developed based on the conceptual and numerical model of Lastras et al. (2005). We have also taken into account all available multibeam bathymetry of the area and high-resolution seismic profiles of the debris flow deposit. The results of the numerical simulation are displayed using plots of snapshots at consecutive times, marigrams of synthetic stations, maximum amplitude plots, and spectral analyses. The obtained outputs show that the nearest shoreline, the Iberian coast, would not be the first one hit by the tsunami. The eastward, outgoing wave would arrive at Eivissa Island 18 min after the triggering of the slide and at Mallorca Island 9 min later, whereas the westward-spreading wave would hit the Iberian Peninsula 54 min after the slide was triggered. This noticeable delay in the arrival times at the peninsula is produced by the asymmetric bathymetry of the Catalano-Balearic Sea and the shoaling effect due to the presence of the wide Ebro continental shelf, which in addition significantly amplifies the tsunami wave (>9 m). The wave amplitudes attain 8 m in Eivissa, and waves up to 3 m high would arrive to Palma Bay. Resonance effects produced in the narrow Santa Ponça Bay in Mallorca Island could produce waves up to 9 m high. A similar event occurring today would have catastrophic consequences, especially in summer when human use of these tourist coasts increases significantly.

Introduction

Tsunami waves are characterized by a long period (minutes to hours) and a long wavelength (hundreds of kilometers), consequently affecting the entire water column, and with a horizontal velocity almost constant from top to bottom. This explains the waves' great momentum, which (i) produces their extreme run-up; that is, their maximum vertical height onshore above sea level is higher than

the height at the coastline; and (ii) gives them the same transport capacity as a four-times-higher storm wave (Bryant 2008). These characteristics are reflected in their catastrophic nature and effects that often produce significant economic damage and even loss of lives; the waves are thus considered an important geohazard (Harbitz et al. 2006). Therefore, the study of potential tsunamigenic sources is key in order to assess the hazard and risk to which a given coastal region is exposed.

In the western Mediterranean Sea, the North African margin is the main tsunamigenic source, an

Manuscript received January 21, 2011; accepted August 8, 2011.

* Author for correspondence; e-mail: glastras@ub.edu.

active margin where convergent motion between the African and European plates has occurred since late Cretaceous (Auzende et al. 1975; Mauffret 2007). Most of the earthquakes epicenters that have generated historical tsunamis in the western Mediterranean were located in this area. The most recent example is the Zemmouri, Algeria, earthquake ($M_w = 6.8$; fig. 1) that occurred May 21, 2003 (Hamdache et al. 2004), which triggered a 2-m-high tsunami registered in the Balearic Islands 40 min after the main shock (Hébert and Alasset 2003; Wang and Liu 2005; Alasset et al. 2006). This archipelago had previously been hit by tsunamis generated by earthquakes in 1856 and 1980, with epicenters in the Algerian margin (Jijel and El Asnam earthquakes, respectively; Soloviev et al. 2000). An assessment of hazard in the Balearic Islands related

to tsunamis generated by the Algerian sources has been recently developed by Álvarez et al (2010).

Seismic activity often triggers submarine landslides, whose tsunamigenic potential has been recently recognized (Pelinovsky and Poplavsky 1996; Rzedkiewicz et al. 1996; Trifunac and Todorovska 2002; Watts et al. 2005), as in the Papua New Guinea (Tappin et al. 1999, 2008; Heinrich et al. 2000; McSaveney et al. 2000; Imamura and Hashi 2002; Watts et al. 2003) or Grand Banks earthquakes in 1929 (Fine et al. 2005). Although there is no conclusive evidence of landslide-generated tsunamis in the North African margin, the relationship between the seismic events of El Asnam and its capacity to trigger submarine landslides was already proposed by El-Robrini et al. (1985).

Submarine landslides are not necessarily linked

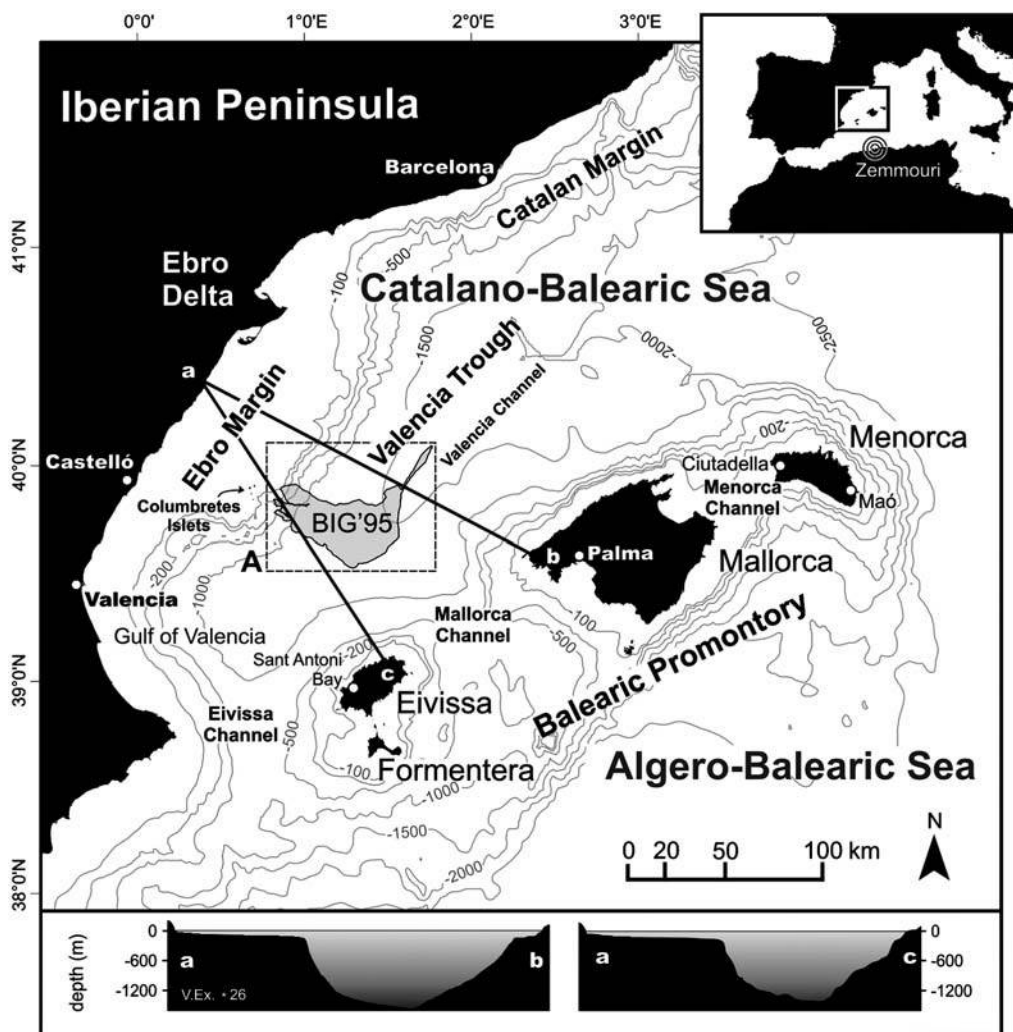


Figure 1. Bathymetric map of the western Mediterranean Sea area around the Balearic Islands. Contours are at 100-, 200-, 500-, 1000-, 1500-, 2000-, and 2500-m water depths. Gray area in box A represents the BIG'95 debris flow deposit. Lines a-b and a-c represent the locations of profiles represented below.

to tectonic activity. Slope instability events with an elevated tsunamigenic potential, such as the Storegga Slide (Bugge et al. 1988; Dawson et al. 1988; Harbitz 1992; Bondevik et al. 2005a,2005b), often occur in passive margins. A steep slope exceeding the internal friction angle, gas hydrate dissociation and/or the presence of free gas in the sediment are common triggering mechanisms of submarine landslides (Canals et al. 2004; Sultan et al. 2004; Masson et al. 2006). Cyclic sediment loading, similar to that produced by a seismic shock, can also be a product of storm waves (or recurrent tsunami waves) generating an excess pore pressure and consequent sediment failure (Lee et al. 2007). Dan et al. (2007) suggest that an increase in pore pressure was the trigger of the submarine landslide that generated the 1979 Nice tsunami in France, for which no seismic activity was recorded (Gennesseaux et al. 1980). It is the only recognized landslide-generated historical tsunami in the western Mediterranean. Similarly, the 2002 tsunami reported in the Rhodes coast, eastern Mediterranean, was attributed to a submarine landslide without any seismic trigger (Papadopoulos et al. 2007).

Moreover, several submarine landslide deposits have been thoroughly found in the Ebro, Catalan, and Balearic margins: among others, the BIG'95 debris flow (Lastras et al. 2002), the four Eivissa Channel (Lastras et al. 2004b) and the two Barcelona slides (Lastras et al. 2007), the Balearic Promontory slides described by Acosta et al. (2003, 2004), and the Torreblanca slide (Casas et al. 2003). These landslides may have acted as nonseismic tsunamigenic sources, and in order to study their tsunamigenic potential, two different approaches can be used: (1) the analysis of similar historical precedents, and (2) the numerical modeling of the process (Skvortsov 2002).

This article presents the analysis of the tsunamigenic potential of the BIG'95 debris flow, in the Ebro continental margin, western Mediterranean (fig. 1), which is the youngest relatively large landslide known in the area (11,500 cal yr BP; Lastras et al. 2002). The analysis is based on the characteristics (slope gradient, volume of deposit, and estimated downslope velocity), as described by Lastras et al. (2002, 2004a, 2005), by applying the Cornell multigrid coupled tsunami numerical model (COMCOT) from Cornell University (Liu et al. 1998). We aim to obtain a present-day, sea-level highstand reasonable scenario for the generation and propagation of the BIG'95 debris-flow-generated tsunami. Propagation and impact of the tsunami waves to nearby coastlines is assessed with regard to arrival times and submarine and coastal

morphology, and especial attention is given to the Balearic coast. This study aims to understand the processes of tsunami generation, propagation and impact in a currently highly populated area, with a long geological record of potentially tsunamigenic submarine landslides, and social and economic factors centered in summer beach tourism that increase tsunami risk in terms of vulnerability and exposure of human lives.

Geological Setting

The Valencia Trough, western Mediterranean Sea, is an extensional basin (Roca et al. 1999) that separates the Balearic Promontory to the southeast and the Ebro and Catalan margins in the Iberian Peninsula to the northwest (fig. 1). The basin is partially closed by the Eivissa channel to the south, and it opens to the northeast into the Provençal Basin (Canals et al. 1982).

The passive terrigenous Ebro continental margin has one of the widest shelves in the western Mediterranean, up to 70 km wide, mainly as a result of the Ebro river sediment input during the Plio-Pleistocene (Nelson and Maldonado 1990). Its steep continental slope (up to 14° in gradient) starts at about 130-m water depth and is cut by several canyon systems (Canals et al. 2000). The architecture of the margin is the result of the interaction between subsiding grabens, glacio-eustatic sea-level oscillations and sediment source controls (Farran and Maldonado 1990). The base of slope is occupied by either incised or filled channel-levee complexes and aprons where sliding, turbidity currents, and hemipelagic settling are the dominant sedimentary processes (Nelson and Maldonado 1988). The Catalan margin to the north has a narrower continental shelf, up to 20 km wide, and is segmented by large submarine canyons incised almost up to the coastline (Amblas et al. 2006; Lastras et al. 2011).

The carbonated Balearic Promontory has a narrow continental shelf (e.g., 10 km on average in Eivissa and 15 km in Mallorca), with the Menorca channel, in between the islands of Mallorca and Menorca, being the only exception. No submarine canyons exist in the northwestern slope of the Balearic Islands. The northeast-trending Valencia Channel, a midocean channel-type submarine valley (Canals et al. 2000), occupies the axis of the Valencia Trough and collects sediments from the bounding margins, funneling them to the Valencia Fan and the Provençal Basin. Given the differences between these margins, the Catalano-Balearic Basin displays a clearly asymmetric morphology (fig. 1). Several magmatic structures are present in the

area, including seamounts and emerged volcanic outbuildings such as the Columbretes Islets, which outcrop in the southern Ebro outer continental shelf (e.g., Maillard and Mauffret 1993; Muñoz et al. 2005).

The BIG'95 debris flow deposit covers 2200 km² of the Ebro continental slope and base of slope at depths ranging from at least 600 to almost 2000 m (Lastras et al. 2002; fig. 1). It has been studied by means of geophysical (swath bathymetry, side-scan sonar, very-high-resolution seismic reflection profiles) and sedimentological (sediment cores, geotechnical analyses) techniques. The deposit volume has been estimated to be at least 26 km³ (Lastras et al. 2002). Although there is no proven triggering mechanism of the debris flow, a set of factors increasing instability in the Ebro region have been suggested, including rapid sedimentation and underconsolidation, seismic activity, and the presence of a buried volcanic dome related to the Columbretes field underneath the deposit (Lastras et al. 2004a).

A conceptual and numerical model of the BIG'95 debris flow was developed by Lastras et al. (2005) in order to describe and characterize the complex sediment dynamics of this particular event. The deposit is divided into four different areas: the source area where the main and secondary scars are located (i), the proximal (ii) and intermediate (iii) areas where blocks of cohesive sediment are found, and the distal depositional area (iv). The model discerned two main sediment types: a totally remolded or loose fraction and a more cohesive one forming blocks. Both phases had a dissimilar dynamic behavior, being the main difference the larger motion capacity of the loose fraction. Whereas runout of the loose material was 110 km, reaching the distal depositional area and stopping after 73 min, blocks reached only the proximal and intermediate areas (at a distance of about 15 km; Lastras et al. 2002, 2005). In the numerical simulations, the loose fraction speed reached 50 m s⁻¹ 8 min after the landslide triggering, while cohesive sediment reached only 20 m s⁻¹.

Methods and Data Set

The COMCOT numerical model has been specifically developed by the Cornell University to simulate tsunamis. It uses the staggered leapfrog finite differences to resolve the shallow water equations (Wang 2006). In addition, this program allows incorporating a time-dependent bathymetry into the equations. This is the main difference between sub-

marine landslide and earthquake-generated tsunami simulations, since in the former, the bathymetry changes gradually during the whole event, and in the latter, movement is considered to be instantaneous. Simulations with COMCOT model take place in different spatial scales, using a nested grid system dynamically coupled.

Therefore, a series of bathymetric grids reflecting seafloor changes during the slide motion have to be constructed as an input for the model (fig. 2A). Grids have been constructed at time steps of 0, 8, 24, 52, and 73 min, coincident with the modeling work by Lastras et al. (2005). Water depth for infinite values of time actually corresponds to the current bathymetry, here used as the final landslide position (fig. 3B), 73 min after the beginning of the slide. Bathymetry data set used in this study is a compilation of several cruises, including BIG'95 (*BIO Hespérides*, 1995), CALMAR (*R/V L'Atalante*, 1997), MATER-2 (*BIO Hespérides*, 1999), MARINADA (*BIO Hespérides*, 2002), and GMO-2 (*R/V Le Suroit*, 2002) surveys, where different models of multibeam acquisition systems were used (Simrad EM12S, EM12D, EM1002, EM12S, and EM300, respectively). Lower-resolution data provided by the Instituto Español de Oceanografía, including topographic data, were used for areas not covered during these surveys.

The bathymetric grid at time 0 represents the water depths before the landslide. This initial bathymetry (fig. 3A) has been prepared by joining bathymetric data from the continental slope surrounding the BIG'95 debris flow headwall and deposit together with inferred isobaths drawn within the landslide limits, as defined by Lastras et al. (2002, 2004a, 2004b, 2005) and Urgeles et al. (2006), and in agreement with the volume of the deposit (26 km³) calculated from very-high-resolution (topographic parametric sonar) seismic reflection data (fig. 2A; Lastras et al. 2002). Resolution of the initial grid is 50 m, so that channels and depressions buried by the debris flow (Lastras et al. 2004a) are represented (fig. 4).

For each intermediate step we consider the characteristic shape of a moving debris flow (Rzadkiewicz et al. 1996; Mohrig et al. 1998; Shanmugam 2000) together with the position of the landslide front and the thickness of the sliding mass obtained from numerical modeling. Slide thickness has been checked to ensure that effective volume, that is, mobilized material that produces a change in the bathymetry, is conserved between consecutive time steps (fig. 2B). The vertical displacement at each cell of the grid is shown in figure 4. Sediment

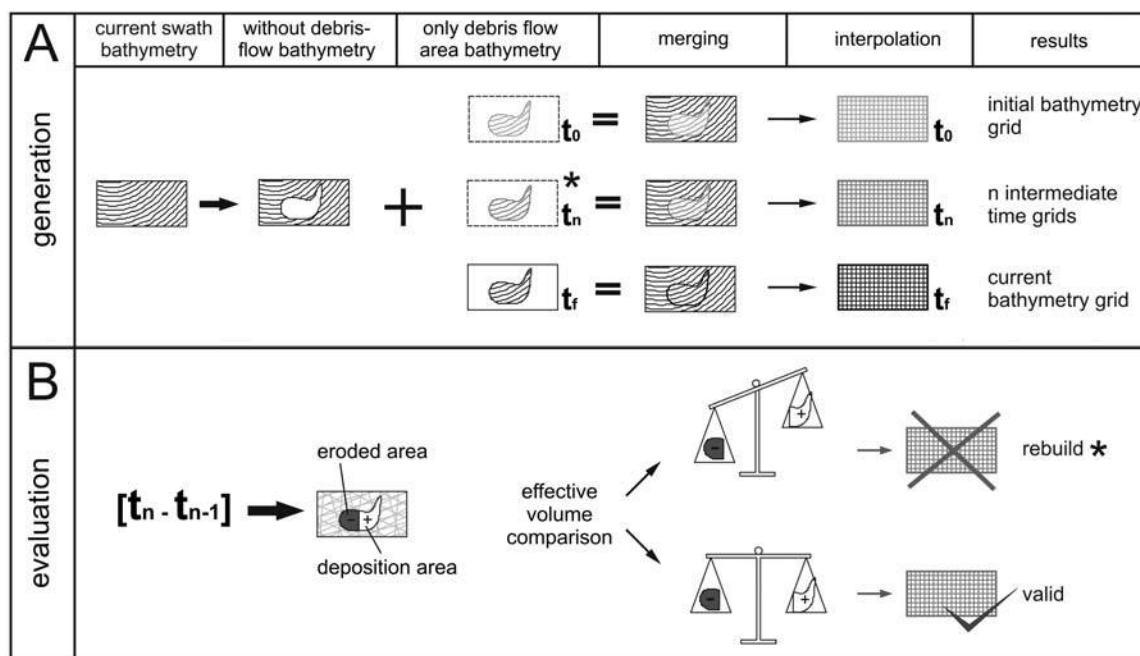


Figure 2. Sketch showing the generation (A) and evaluation (B) of time-step bathymetric grids (limited by box A in fig. 1) used as an input to the model. Term t_0 is the initial bathymetry, t_f is the present-day bathymetry; intermediate time-steps are t_n ($0 < n < f$). Grids are evaluated by checking the eroded and deposited volumes with respect to the prior time-step sum zero. If the volumes are incongruent we rebuild the debris flow area bathymetry at this time-step (t_n). Isobaths files are represented as lines and grids as squares. Available data are represented in black and constructed data in light and dark gray for initial bathymetry and time-step grids, respectively.

that occupies a volume previously also occupied by sediment in two consecutive time steps does not account any change in bathymetry, and thus is ineffective in terms of tsunami generation (Trifunac and Todorovska 2002). Effective volume calculated for the BIG'95 debris flow is 17 km^3 , which is 66% of the total landslide mass.

Each bathymetric grid, the initial, intermediate, and final time steps (fig. 5), has been integrated in a larger grid of the study area (zone 1, 200-m cell size) that also includes the topography of the adjacent mainland and the Balearic Islands (fig. 6). All grids have been projected in Cartesian coordinates (UTM 31N, WGS-84). COMCOT model allows improving the resolution of the output in specific areas through grid nesting. We have used two secondary grids: zone 2 (100-m cell size, nested in zone 1), centered in the continental shelf, slope, and rise offshore Palma Bay; and zone 3 (50-m cell size, nested in zone 2), focused in Palma Bay (fig. 6). Grid cell sizes and computing time step (0.5 s) were chosen to satisfy the Courant condition; that is, the time interval used is shorter than the time required for the wave to cross a spatial cell, in order to make the computations stable and avoid generation of

erroneous small-scale oscillations. The total duration of the simulation is 9000 s so that it includes the whole landslide motion (4380 s) and extra time for the visualization of the propagating waves.

Results

The output of the simulation of the BIG'95 landslide-generated tsunami allows to measure free water surface changes at any point along time. The height wave plots show that the landslide produces a dipole wave with a trough (blue in fig. 7) located over the sediment source area in the upper slope and an adjacent crest (red in fig. 7) to the southeast.

This initial wave radially spreads, and progressively becomes deformed, acquiring an ellipsoidal shape whose major and minor axes are northeast-southwest and northwest-southeast, respectively. The northwestern covertex is formed by a tsunami wave train that advances toward the Iberian Peninsula at a significantly slower speed, with a greater amplitude and a smaller wavelength than the outgoing wave, which is directed toward the Balearic Islands. The outgoing wave would impact the coast of Eivissa Island 18 min after the triggering of the

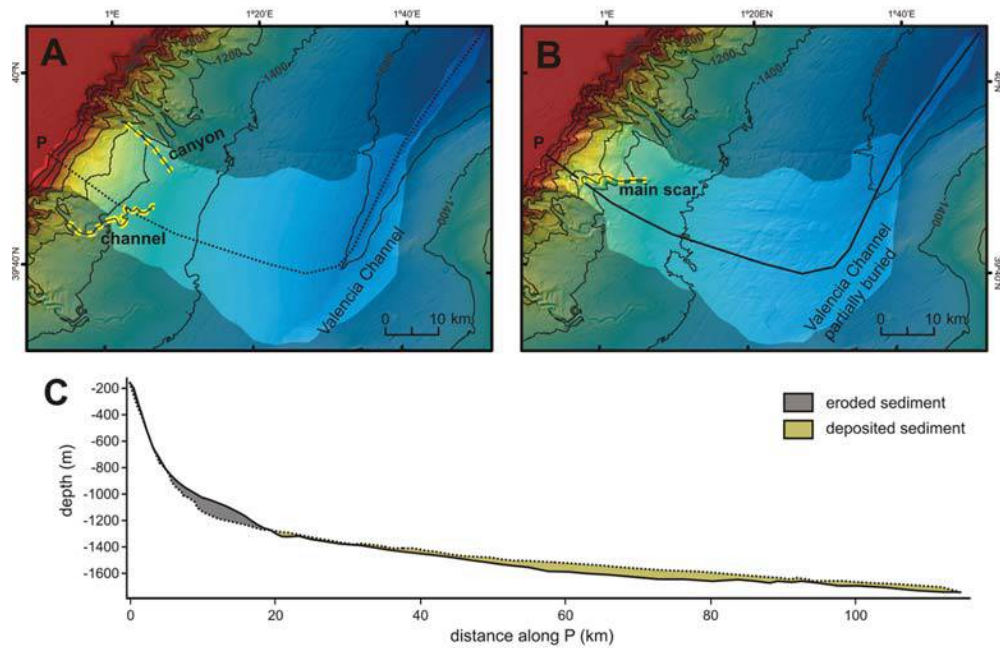


Figure 3. Initial (A) and current (B) bathymetry of the BIG'95 debris flow area (box A in fig. 1). Isobaths every 200 m. Dashed yellow lines represent linear morphological elements that evidence temporal changes: buried channels (in A) and scars (in B) left by the debris flow. Depth profile (C) shows the difference between both bathymetries along line P. Dashed line corresponds to the initial profile, and the continuous line to the present-day one.

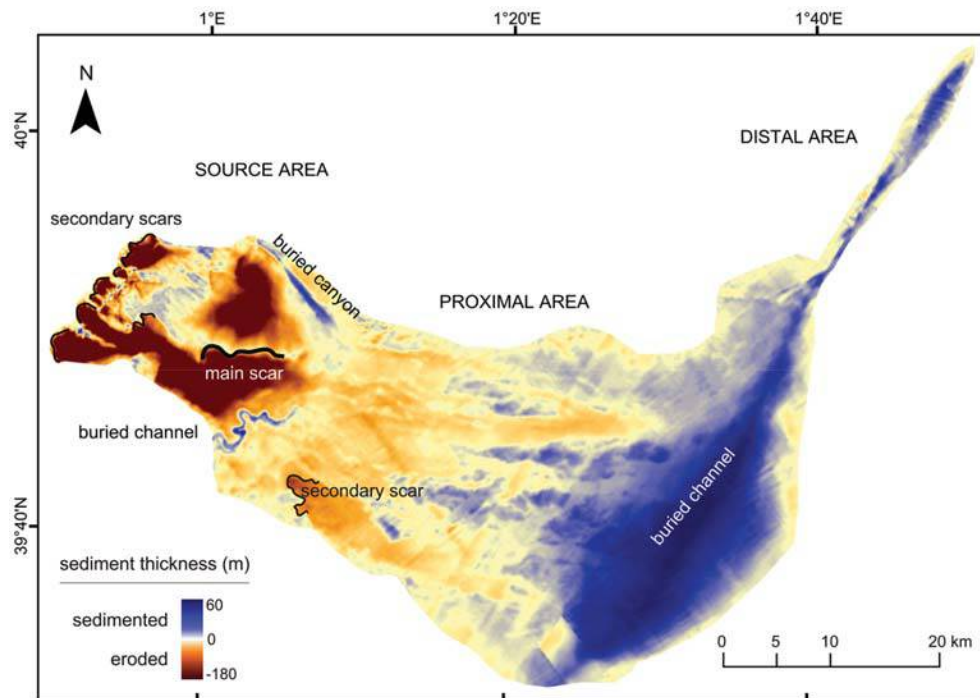


Figure 4. Erosion-deposition plot of the BIG'95 debris flow, resulting from subtracting the final bathymetry from the inferred one previous to the slide. The value of each cell is the thickness of material either eroded (brown) or sedimented (blue).

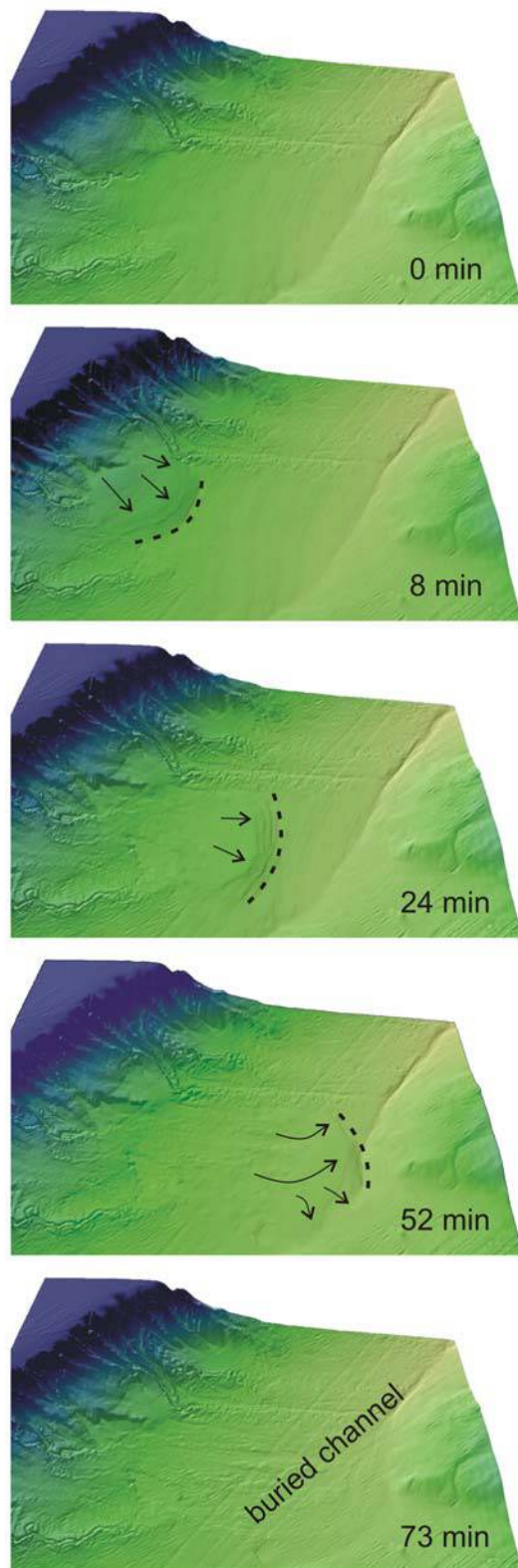


Figure 5. Reconstruction of the BIG'95 debris flow movement (*box A* in *fig. 1*) used for tsunami simulation at five consecutive time steps. The initial time at 0 min

landslide and reach Mallorca Island 9 min later (27 min since the initial trigger). The slower back-going tsunami wave would arrive to the Iberian Peninsula 54 min after the initiation of the landslide, first reporting a negative amplitude (*fig. 7*). The plots of the nested Palma Bay grids (zones 2 and 3 in *fig. 6*) show the wave already into Palma Bay 44 min after the landslide was triggered and hitting the coast inside the bay before 60 min (*fig. 8*), with an amplitude of between 2 and 3 m.

Wave amplitudes can be analyzed by using synthetic marigrams. These have been calculated along a computation time of 150 min at five different stations (*fig. 9*), two above the source area (stations 1 and 2, 900 and 1250-m water depth, respectively; *fig. 9*) and three near the coastlines north of Eivissa (station 3, 10-m water depth; *fig. 9*), west of Mallorca (station 4, 10-m water depth; *fig. 9*), and in front of the city of Castelló in the Iberian Peninsula (station 5, 10-m water depth; *fig. 9*). The sea-level perturbation caused by the BIG'95 debris flow forms a trough up to 4 m deep in station 1 and a crest up to 2 m high in station 2, with periods of 10 to 15 min in both near-field stations (*fig. 9*). Ten minutes later, station 2 shows a drop in the free surface of 3 m. Approximately at the same time, station 1 shows an increase of the free surface that reaches 5 m high, with similar periods. After that, only minor disturbances are observed.

Free surface at far-field station 3 remains at rest until around 18 min after the landslide. At that time, a wave crest up to 8 m high with a first period of 10 min arrives, followed by a sea level drop of almost 4 m. This implies a free surface change of nearly 12 m in less than 5 min. The same first crest arrives at the Mallorca coast after 27 min, with amplitudes up to 4 m in height at far-field station 4. The highest wave recorded in these coastal stations reaches Castelló 64 min after the triggering of the landslide, and is 9 m high and around 25 min in period. This maximum height is preceded by a 6 m deep trough arriving after 54 min, yielding a total 15 m of free surface change.

Using the maximum resolution grid (zone 3 in *fig. 6*), six other stations have been computed in and around Palma Bay above <10-m water depth (*fig. 10*). The amplitudes of the waves arriving to Palma Bay are approximately 3 m high in all the stations for the first crest, with periods between 10

represents the bathymetry before the slide, while times 8, 24, and 52 min are intermediate times and time 73 min corresponds with the present-day bathymetry. View is from the south.

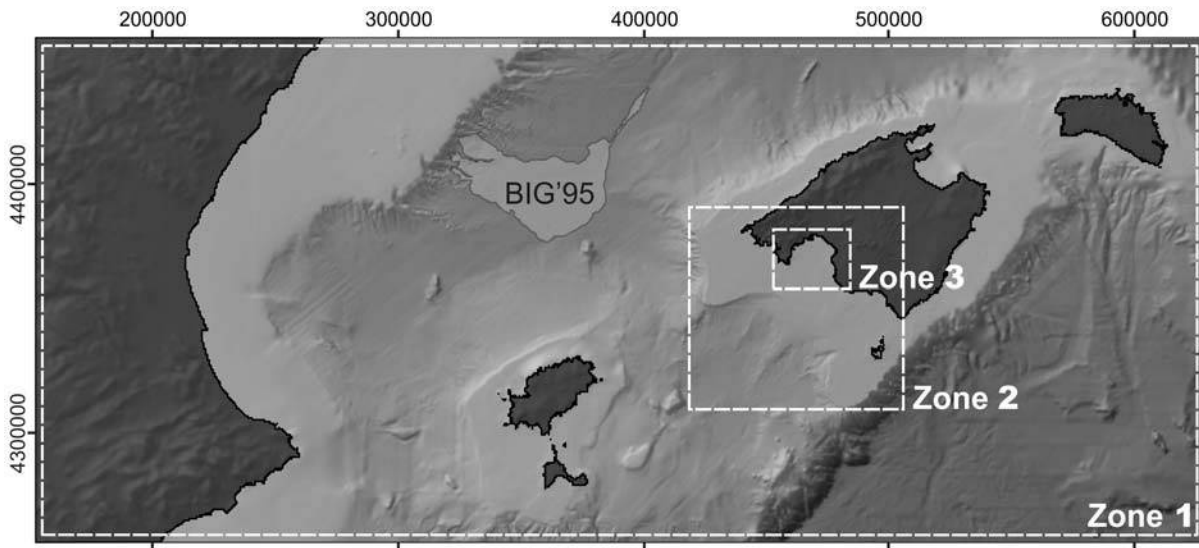


Figure 6. Extension of the nested grids of bathymetry and topography integrated data. Zone 1 covers $\sim 10^5$ km²; zone 2, $\sim 7 \times 10^3$ km²; and zone 3, $\sim 7 \times 10^2$ km². The resolutions of the grids are 200, 100, and 50 m, respectively. See figure 1 for location and feature names.

and 15 min. Maximum amplitudes of more than 3 m are reached in Sa Torre and Palma stations 55 and 60 min, respectively, after the beginning of the slide. The computed station at Santa Ponça Bay (fig. 10) registers the maximum amplitude observed in the simulation, with a height of up to 9 m impacting 44 min after the event start. Subsequent oscillations exceed 2 m in height during 2 h after the first arrival.

Wave spectra of the time series of zone 1 stations have been obtained using the fast Fourier transform (fig. 11). The graphic shows that the station with higher energy content is Castelló station (point 5 in fig. 9) with its energy concentrated at lower frequencies (30-min period). The other spectra have a lower energetic content concentrated at higher frequencies. The highest value at high frequencies (between 5 and 15 min) was obtained in the Eivissa station. Despite difference in energy content, the main oscillation periods match in all five stations (fig. 11).

The maximum elevations plot (fig. 12) shows the maximum free surface elevation reached at each cell in zone 1 during the complete simulation run. Values range from 0 to 10 m, with the lowest ones located in the Algero-Balearic Sea and Provençal Basin, in the southwestern part of the Valencia Trough and in the western part of the Eivissa Channel. Mean elevations of <1 m, with peaks of up to 2–3 m are observed near certain coastlines, such as the southern part of Gulf of Valencia and the northern and southern shores of Mallorca Island. Mean

elevations <2 m with peaks of up to 6–7 m are reached in the surrounding areas of the Mallorca westernmost coast and around Formentera Island. Mean elevations of >3 m are observed in two large areas above the Valencia Trough, one extending over the depositional area of the debris flow deposit and the northern Eivissa coast, and a second one over the source area of the debris flow and the eastern coast of the Iberian Peninsula. The later one, which includes large areas of the continental shelf of the Ebro margin, is characterized by the highest values recorded, mostly over 8 m.

Discussion

The wave generated by a submarine landslide such as the BIG'95 debris flow mainly depends on the volume and mass of the landslide, its depth, the slope angle of the sliding surface, and the speed of the landslide movement, with the volume and the velocity being the most important (Pelinsonsky and Poplavsky 1996; Papadopoulos and Kortekaas 2003; Harbitz et al. 2006). Knowledge of most of these parameters can be attained using geophysical methods, and the velocity of the slide is generally inferred from numerical modeling or by indirect evidence (e.g., timing of successive submarine cable breaks). The combination of all these factors makes it difficult to set the threshold value for each of these parameters at which a submarine landslide becomes tsunamigenic.

The tsunamigenic character of the BIG'95 debris

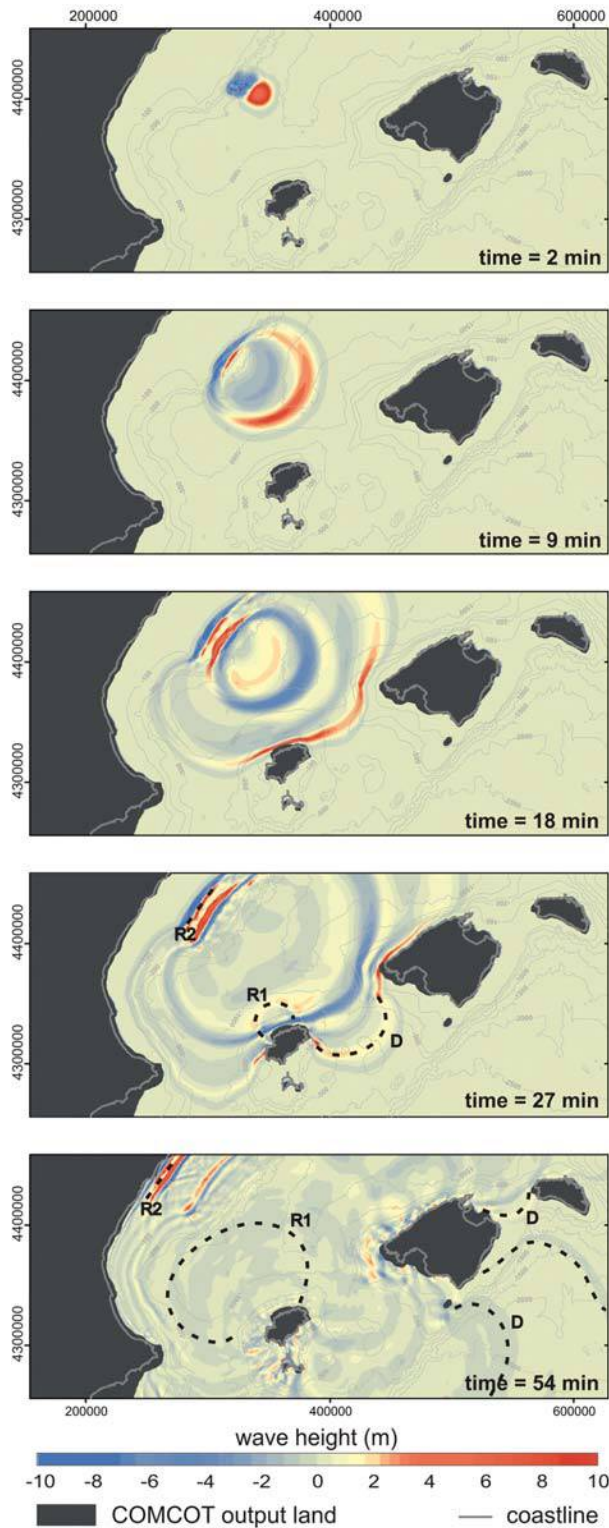


Figure 7. Height of the generated tsunami wave at different times, computed for zone 1 (see fig. 6). The first snapshot shows the generation of the tsunami wave and

flow event was demonstrated in “Results,” and the parameters of this landslide are consistent with those of some historic tsunamigenic submarine landslides. For instance, the volume involved in the failure that generated the 1998 Papua New Guinea tsunami, which caused 2200 deaths, was 6.3 km^3 , and its estimated velocity was 35 m s^{-1} (Tappin et al. 2008), values smaller than the 26 km^3 (17 km^3 of effective volume) and the 50 m s^{-1} of the BIG’95 debris flow. The 3–11-m-high recorded tsunami in Skagway (Alaska) in 1994, triggered by a landslide $3 \times 10^6 \text{ m}^3$ in volume (Kulikov et al. 1996; Rabinovich et al. 1999; Watts et al. 2003), and the 11-m-high Nice (France) tsunami in 1978, produced by a $0.8 \times 10^6 \text{ m}^3$ landslide (Genesseeux et al. 1980; Assier-Rzadkiewicz et al. 2000) occurred at much shallower water depths. Tsunami height values obtained in sites with source landslides located on the upper continental slope, as in the BIG’95 debris flow case, are more similar to and of the same order of magnitude as those computed in our study, as in the case of the Currituck landslide (Geist et al. 2008) or the 1918 Mona Passage (Puerto Rico) landslide (López-Venegas et al. 2008), which resulted in tsunamis 1.2–8.8 m and up to 5 m high, respectively. In the Mediterranean, the 1956 South Aegean Sea tsunami reached 20 m in height in the eastern coasts of Amorgos Island, Greece (Okal et al. 2009). Such a run-up has been related to the combination of an $3.6 \times 10^6 \text{ m}^3$ slump in the upper slope and both fore- and aftershock events (Perissoratis and Papadopoulos 1999), and thus it can not be considered a pure landslide-generated tsunami.

The computed tsunami in our study has the common characteristics of a tsunami generated by a submarine landslide, consisting of a rounded dipole with a leading elevation phase originated on the region of deposition and a leading depression phase above the source area (fig. 7; Fine et al. 2005; Rahiman et al. 2007). This contrasts with the elongated dipoles generated by earthquakes that hinder the fast radial damping characteristic of the

its spread. At 18 min the tsunami wave is arriving at the northern coast of Eivissa. At 27 min, it hits the westernmost coast of Mallorca, and at 54 min, the wave train is hitting the Castelló coast on the Iberian Peninsula. The dark gray areas are considered emerged land by the model, and thereby output data for water-free surface calculations is lacking. The light gray lines superimposed on these areas represent the current coastline. R1, R2, and D show the wave reflection, refraction, and diffraction, respectively. COMCOT = Cornell multigrid coupled tsunami model.

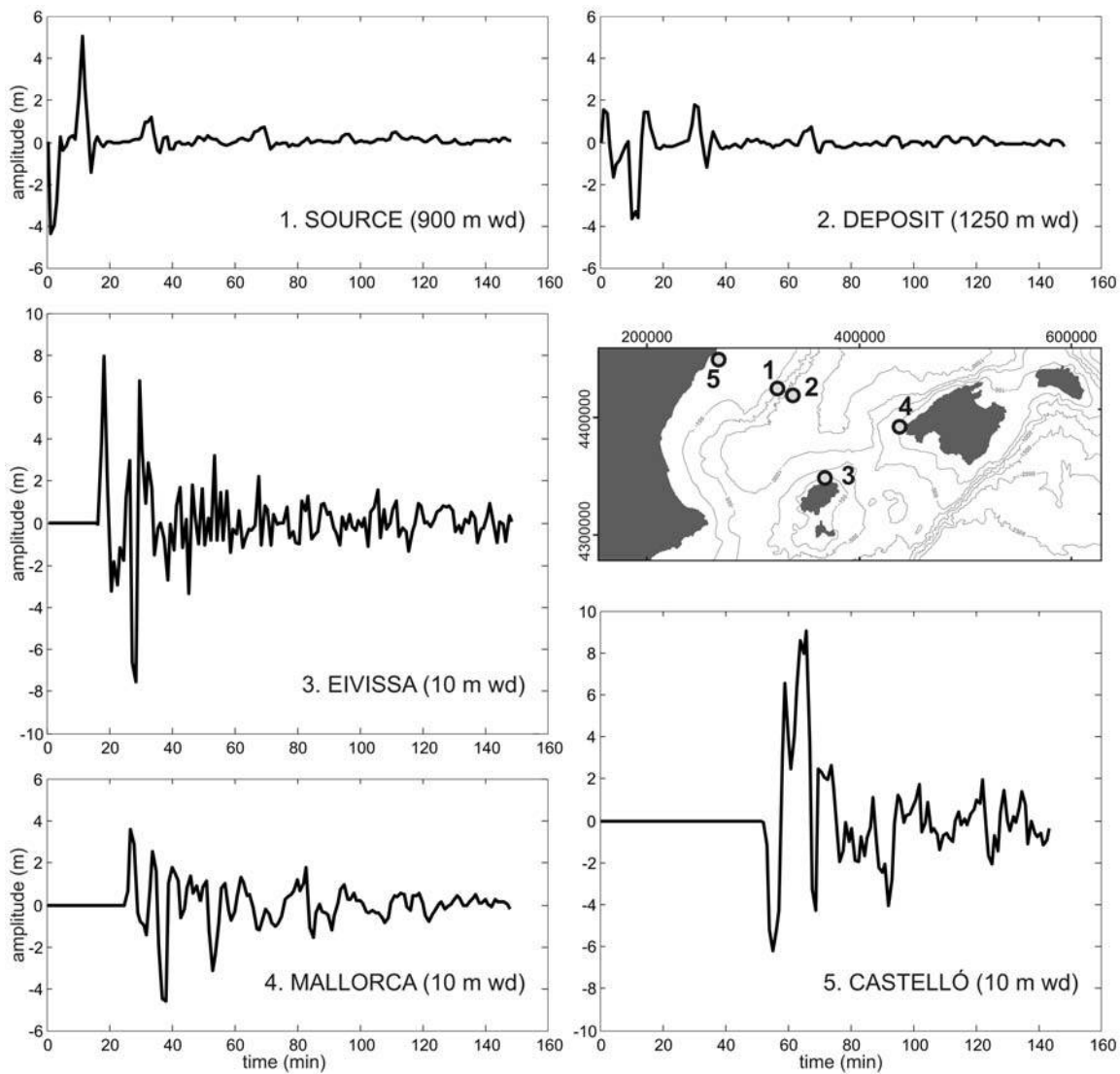


Figure 9. Computed marigrams above the tsunami source (1, 2), off north Eivissa (3), off Palma Bay (4), and off Castelló (5); wd = the water depth over which each station is located (see inset for location). Note the different arrival times, periods, wave heights, and polarities.

rounded or punctual sources. Their rounded geometry can explain the accentuated effects of these kinds of tsunami triggers (Harbitz et al. 2006), being the type of the source a key point to assess the energetic behavior of a given event.

This behavior is also heavily dependent on the propagation of the tsunami wave and its approach to the coast as it is modified by the morphology of the seabed. Thus, the resolution of bathymetric data plays a critical role in simulation studies. In our simulation, the back-going tsunami waves reach the Ebro continental shelf edge, which produces a wave refraction (R2 in fig. 7). Due to this refraction, the wave front becomes parallel to the

bathymetric lines. Moreover, the <130-m-deep Ebro shelf produces a strong shoaling effect that, in addition to delaying the arrival of the wave train to the coast, significantly increases the amplitude of the waves, explaining the large area with elevated maximum height values in the amplitude plot (fig. 12).

Outgoing wave speed, amplitude, and length depend on the direction of the front. Outgoing waves directed to the northeast are the fastest, due to the increase in depth towards this direction, corresponding to the Valencia Channel axis (fig. 7). The wave front directed to the southeast, which matches with the landslide movement, have higher

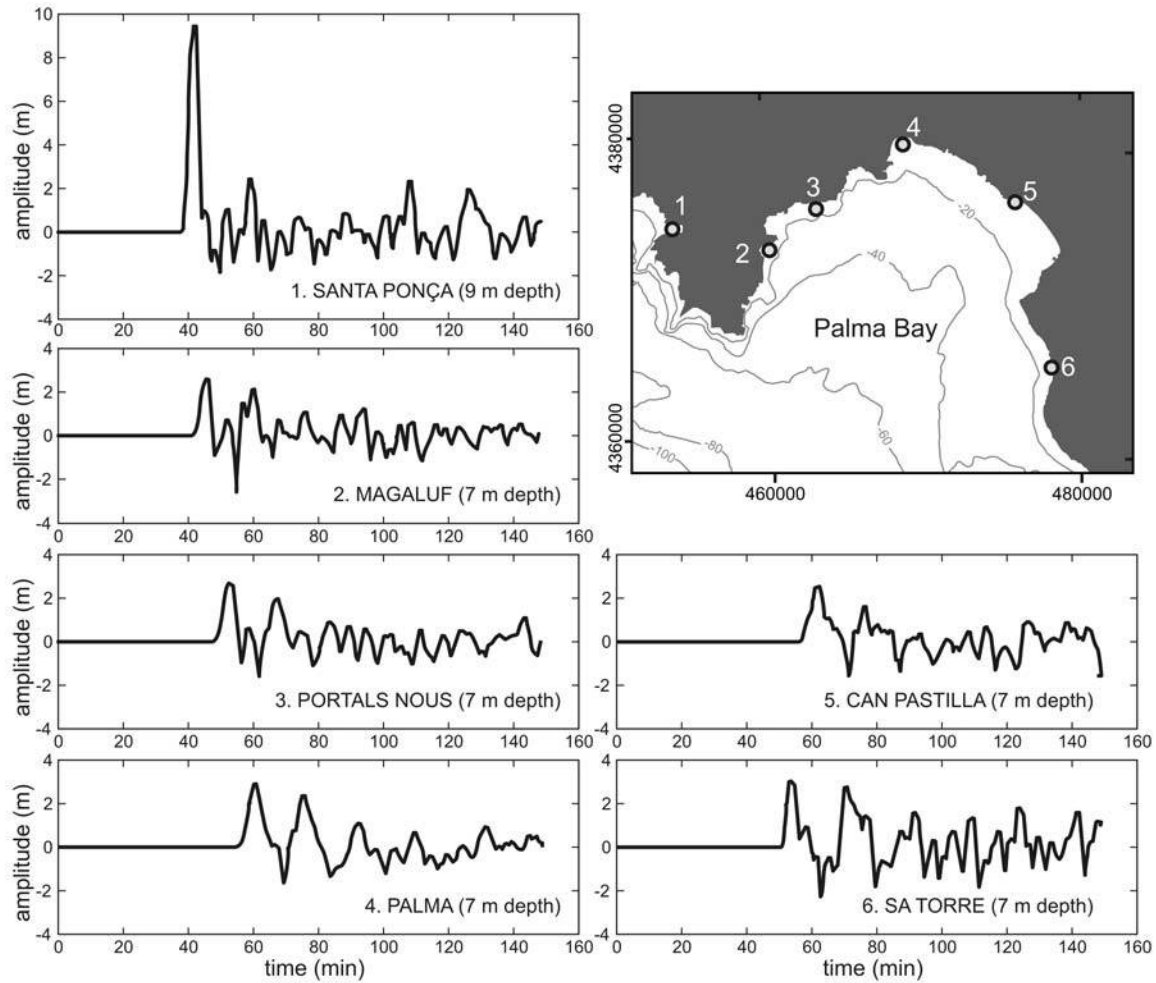


Figure 10. Computed marigrams of six synthetic coastal stations in zone 3 (see fig. 6). Maximum amplitudes reached are up to 3 m high in Palma Bay (points 2–6) and up to 9 m in Santa Ponça Bay; wd = the water depth of each station (point 1; see also fig. 8 at 44 min).

amplitudes (fig. 12). This front encounters two obstacles in its propagation: Mallorca and Eivissa Islands, which produce both reflection and diffraction effects. The reflected waves develop over the exposed side of the islands, and spread back to the Catalano-Balearic Sea (R1 in fig. 7). Diffraction, in contrast, is produced between the topographic obstacles, as in the Eivissa and the Mallorca channels (D in fig. 7), where two new, weaker wave fronts develop. Mallorca Island is large enough to create a shadow zone that prevents the arrival of significantly high waves to its leeward side. This shadow zone includes Menorca Island and the southeastern coast of Mallorca. However, the obstacle effect of the Eivissa Island is much smaller, and Formentera and the southern Eivissa coast are unprotected against the effects of the diffracted wave front. This is in agreement with the records of the earthquake-

generated tsunami from North Africa that hit the area on May 23, 2003. During this event, the shadow zones of Mallorca and Eivissa islands, located leeward in relation to the source (Zemmouri, Algeria; fig. 1), received a different tsunami impact: low amplitudes, if any, were recorded north of Mallorca, whereas damages were reported in the northern coast of Eivissa (i.e., Sant Antoni Bay; fig. 1; Alasset et al. 2006).

The differences in amplitude recorded along the coast covered in our study show the importance of local studies, proving that due to the basin configuration and the coastal morphology, some regions are much more susceptible to tsunami flooding than others during the same event. Moreover, each site has local characteristic oscillations defined by the topography and bathymetry of the corresponding coast and the adjacent shelf (Marcos et al. 2009).

Where the natural period of oscillation of a bay or port matches with the incident tsunami wave train period, amplification or resonance phenomena may occur, notably increasing the destructive capacity of the wave. In Balearic harbors such as Maó and Ciutadella (Menorca; fig. 1), resonance effects often occur due to atmospheric gravity waves known as seiches (Monserrat et al. 1991), which have caused important damage in historic times. A similar effect could be produced by tsunami waves (Otero 2008), whose period is similar to that of atmospheric gravity waves typical in this region. These cannot be observed in our study, since these ports are located at the shadow zone with respect to the BIG'95 debris flow, where no significant amplitudes were obtained and not enough grid resolution is available to study these local effects. Nevertheless, grid size of zone 3 allows observing that no resonance effects are induced in Palma Bay by the leader waves generated. Its wave periods (10–15 min) are smaller than the natural oscillation of Palma Bay, between 17 and 20 min (TRANSFER 2009). However, coastal features such as small bays with natural oscillation periods smaller than 10 min can generate resonance effects (e.g., Santa Ponça; fig. 10). Periods of tsunamis generated by Algerian coast seismic sources (Alvarez et al. 2010) are larger than those generated by submarine landslides.

Wave spectra usually have a strong variability due to local bottom morphology, causing the same tsunami event to yield different spectral outputs for each station, as in the case computed for the BIG'95 tsunami (fig. 11). The common general characteristics in the oscillation periods are the signature of this specific source. The wave spectrum of Castelló station differs from the rest mainly at low frequencies (long periods), related to local topography and its major effect on long wave oscillations at Castelló site. The prominent peak at 30 min in that station (fig. 11) could be caused by resonant excitation of trapped edge waves on the Ebro shelf, since resonance effects on the shelves often occur at low frequencies (Abe 2001; Pelinovsky et al. 2009; Ivelskaya et al. 2010). The low energy content in the spectra of both source and deposit stations is due to the distance to the coast, which prevents any resonance effects.

Numerical simulations also yield important information on wave arrival time at different locations, which is only dependent of the bathymetry. High-resolution data sets are necessary to estimate realistic arrival times. In our study area, the difference in arrival times would give very little leeway (only ~37 min) to forecast and warn about the

tsunami arrival at the Iberian Peninsula once it had been reported in Eivissa coasts.

The large urban concentrations and infrastructures in our study area are located mainly along the coastline, particularly in the case of the Balearic Islands, which have a high dependence on maritime communications. Moreover, the local economy is centered in summer tourism, which tends to locate facilities and buildings on the coast. This produces a large hourly and seasonal variation in population exposure at the shore, which could be very elevated during beach hours on summer. High exposure to a potential tsunami affecting the coast entails a high vulnerability and, therefore, an elevated risk for these communities. Risk also depends on hazard and therefore on tsunami frequency (i.e., its recurrence interval; ten Brink et al. 2009). Although no landslide recurrence studies are available for the Catalano-Balearic Sea, at least two major mass wasting deposits are embedded within the Plio-Quaternary sequence in the BIG'95 debris flow area as seen in seismic reflection profiles (Lastras et al. 2004a), which sum up to several smaller landslide deposits observed throughout the Valencia Trough (Lastras et al. 2007). The lack of precise dating of such deposits prevents establishing a realistic recurrence time for landslide events in the Catalano-Balearic Sea.

Short earthquake records available in the North African margin avoid inferring an accurate recurrence time for seismic events, although Swafford and Stein (2007) infer a 95-yr mean recurrence for $M_w \geq 7$ events in the area. Tsunami watch and warning statements are issued by NOAA/WEST Coast and Alaska Tsunami Warning Center when an earthquake exceeds the threshold magnitude that has been calculated for a given area, using the historical record (Whitmore et al. 2009). Given that El Asnam ($M_w = 7.3$) and Zemmouri ($M_w = 6.9$) earthquakes were tsunamigenic, similar $M_w \geq 7$ events could be considered as probably tsunamigenic, thus yielding an inferred tsunami recurrence time of 95 yr. Although this earthquake-generated tsunami recurrence time is much shorter than the landslide-generated tsunami one, the later can be much larger, at least if we compare the computed BIG'95 generated tsunami with either the measured one produced by the Zemmouri earthquake or the simulated for other North African earthquakes (TRANSFER 2009; Alvarez et al. 2010).

Urgeles et al. (2006) have calculated that the present-day slope in the BIG'95 debris flow area is safe (factor of security 1.77) and that a pseudostatic acceleration of almost 0.1 g is needed to promote further failure; thus, the potential of such an event at

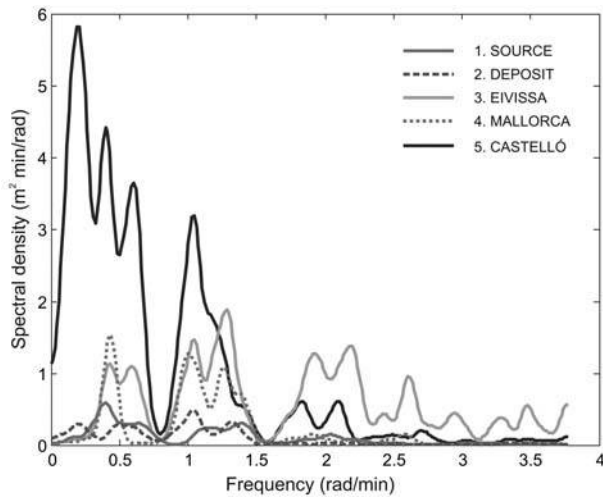


Figure 11. Spectral analysis of synthetic marigram stations of figure 9. The largest peaks are located at low frequencies, especially at Castelló station, that present the largest energy at 0.3 rad min^{-1} (30 min).

present is low in the absence of a significant earthquake shock. Nevertheless, it should be noted that the BIG'95 debris flow is not the only mass-wasting event identified in the Valencia Trough, and several, although smaller, landslide masses whose tsunami potential is yet to be investigated have been identified throughout (Lastras et al. 2007).

The BIG'95 debris flow deposit has been dated to have occurred at prehistoric times (Lastras et al. 2002), and the generated tsunami has been simu-

lated in this work in present-day conditions. At that time, sea level was located $\sim 40\text{--}50 \text{ m}$ below the present sea level (Lambeck and Bard 2000; Lambeck et al. 2011). Obviously, this caused coastlines to be located at a shorter distance from the current continental shelf edge than at present. The generated wave above the source and depositional areas would not be different from that simulated under present-day conditions, since water depth differences between the two periods would be $<4\%\text{--}5\%$ at 1000 m water depth. Thus, the BIG'95 debris flow would also be tsunamigenic in prehistoric sea-level conditions, but its effects should be somehow different taking into account that (1) a smaller shoaling effect would exist on the Iberian coast, but (2) the coast would be located closer to the source area and dissipation of the wave would be minor with respect to current-day conditions.

Conclusions

Using the COMCOT tsunami model, we have demonstrated that the 11,500 cal yr BP BIG'95 submarine debris flow in the western Mediterranean was capable of triggering a local tsunami. The landslide would produce a rounded dipole tsunami wave with a negative back-going wave directed toward the Iberian Peninsula and a positive outgoing wave toward the Balearic Islands. This rounded dipole is in agreement with that expected from a point-source generated tsunami, in contrast to elongated dipoles generated by line-source generated tsu-

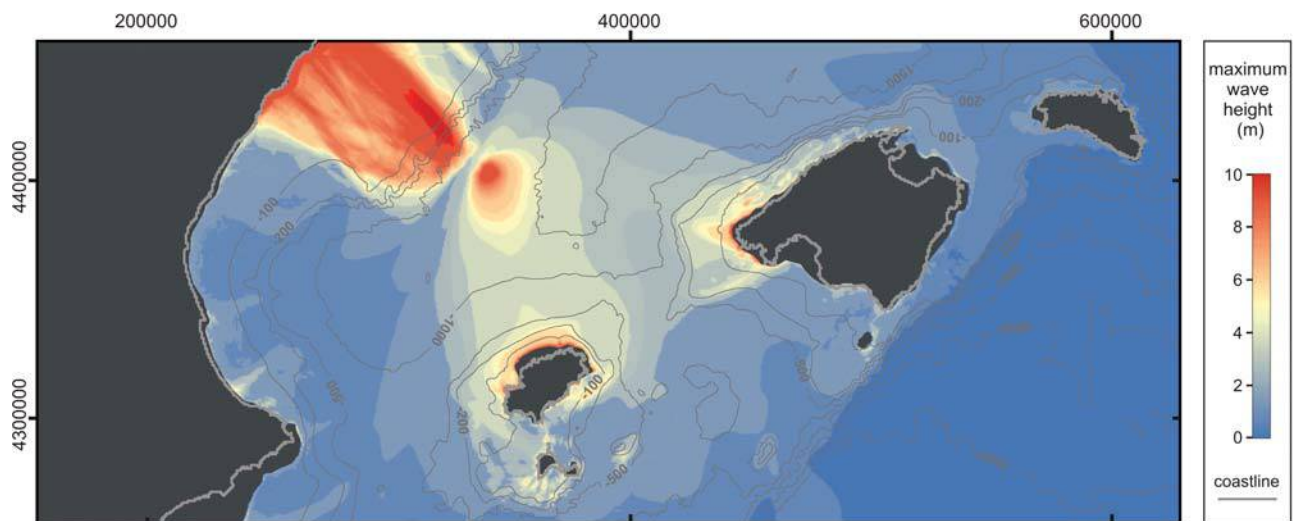


Figure 12. Maximum free surface elevation plot reached at each point of zone 1 (see fig. 6). Highest values (red) are mainly located over the Ebro Margin continental shelf. See figure 1 for place and feature names.

nami, such as those triggered by earthquakes (e.g., movements along a linear fault).

In a present-day scenario, the first wave arrival would occur in the northern coast of Eivissa Island 18 min after the triggering. A strong shoaling effect produced by the presence of the Ebro continental shelf would increase wave height (up to 9 m) and delay arrival time to the Iberian Peninsula (54 min since triggering). The period of the leading waves, between 10 and 15 min, would produce resonance effects in little bays with natural oscillation periods shorter than 10 min, notably increasing wave amplitude (up to 9 m in Santa Ponça Bay).

The presence of the Mallorca and Eivissa islands, which are obstacles for the wave spreading, produce both wave reflection and diffraction effects. Mallorca Island is large enough to create a protected shadow area to its southeast, whereas Eivissa Island does not produce such an effect, and its leeside coasts, together with Formentera coasts, could be hit by the stronger diffracted front wave.

Numerical simulations are a useful tool to assess tsunami hazard in places where local bathymetry and topography could amplify considerably the wave effect, as well as delay the wave arrival to the coast. In order to obtain high quality simulations,

a good assessment of both bathymetry and landslide parameters is required.

ACKNOWLEDGMENTS

This research was supported by the TRANSFER project, European Commission (EC) contract 037058-TRANSFER funded by the EC's Sixth Framework Programme, GRACCIE-CONSOLIDER project (ref. CSD2007-00067) of the Spanish Plan Nacional I+D+I, and a Generalitat de Catalunya "Grups de Recerca Consolidats" grant (2009 SGR 1305). O. Iglesias and R. Durán are supported by an FPU fellowship of the Spanish Ministerio de Educación and a Juan de la Cierva fellowship of the Spanish Ministerio de Ciencia e Innovación, respectively, and E. Tahchi is supported by a Marie Curie Intra-European Fellowship. We would also like to thank all scientists and crew who participated in seagoing activities to obtain geophysical data. We thank G. Papadopoulos, an anonymous reviewer, and the editor for their thoughtful revisions. RTD projects that funded the cruises are also acknowledged. The publication reflects only the views of the authors. The EC is not liable for any use that may be made of this article.

REFERENCES CITED

- Abe, K. 2001. Exclusion of a coastal effect from tsunamis recorded at ports in the use of the observed seiche. International Tsunami Symposium 2001 (Seattle) proceedings, Tsunami Society, p. 611–618.
- Acosta, J.; Canals, M.; Carbó, A.; Muñoz, A.; Urgeles, R.; Muñoz-Martín, A.; and Uchupi, E. 2004. Sea floor morphology and Plio-Quaternary sedimentary cover of the Mallorca Channel, Balearic Islands, western Mediterranean. *Mar. Geol.* 206:165–179, doi:10.1016/j.margeo.2004.02.008.
- Acosta, J.; Canals, M.; López-Martínez, J.; Muñoz, A.; Herranz, P.; Urgeles, R.; Palomo, C.; and Casamor, J. L. 2003. The Balearic Promontory geomorphology (western Mediterranean): morphostructure and active processes. *Geomorphology* 49:177–204, doi:10.1016/S0169-555X(02)00168-X.
- Alasset, J. P.; Hébert, H.; Maouche, S.; Calbini, V.; and Meghraoui, M. 2006. The tsunami induced by the 2003 Zemmouri earthquake ($M_w = 6.9$ Algeria): modelling and results. *Geophys. J. Int.* 166:213–226, doi:10.1111/j.1365-246X.2006.02912.x.
- Álvarez, J. A.; Olabarrieta, M.; González, M.; Otero, L. J.; and Carreño, E. 2010. The impact of tsunamis on the island of Majorca induced by north Algerian seismic sources. *Turk. J. Earth Sci.* 19:367–383, doi:10.3906/yer-0812-7.
- Amblas, D.; Canals, M.; Urgeles, R.; Lastras, G.; Liqueste, C.; Hughes-Clarke, J. E.; Casamor, J. L.; and Calafat, A. M. 2006. Morphogenetic mesoscale analysis of the northeastern Iberian margin, NW Mediterranean Basin. *Mar. Geol.* 234:3–20, doi:10.1016/j.margeo.2006.09.009.
- Assier-Rzadkiewicz, S.; Heinrich, P.; Sabatier, P. C.; Savoye, B.; and Bourillet, J. F. 2000. Numerical modelling of a landslide-generated tsunami: the 1979 Nice event. *Pure Appl. Geophys.* 157:1707–1727, doi:10.1007/PL00001057.
- Auzende, J. M.; Bonnin, J.; and Olivet, J. L. 1975. La marge nord-africaine considérée comme marge active. *B. Soc. Geol. Fr.* 17:681–690.
- Bondevik, S.; Løvholt, F.; Harbitz, C.; Mangerud, J.; Dawson, A.; and Inge, S. J. 2005a. The Storegga Slide tsunami: comparing field observations with numerical simulations. *Mar. Petrol. Geol.* 22:195–208, doi:10.1016/j.marpetgeo.2004.10.003.
- Bondevik, S.; Mangerud, J.; Dawson, S.; Dawson, A.; and Lohne, Ø. 2005b. Evidence for three North Sea tsunamis at the Shetland Islands between 8000 and 1500 years ago. *Quaternary Sci. Rev.* 24:1757–1775, doi:10.1016/j.quascirev.2004.10.018.
- Bryant, E. 2008. *Tsunami: the underrated hazard* (2nd ed.). Berlin, Springer, 336 p.
- Bugge, T.; Belderson, R. H.; and Kenyon, N. H. 1988. The

- Storegga slide. *Philos. Trans. R. Soc.* 325:357–388, doi:10.1098/rsta.1988.0055.
- Canals, M.; Casamor, J. L.; Urgeles, R.; Lastras, G.; Calafat, A. M.; De Batist, M.; Masson, D.; Berné, S.; Alonso, B.; and Hughes-Clarke, J. E. 2000. The Ebro continental margin, western Mediterranean Sea: interplay between canyon-channel systems and mass wasting processes. *In* Nelson, C. H., and Weimer, P., eds. *Deep-water reservoirs of the world*. Gulf Coast Section SEPM Foundation Annual Research Conference, 20th (Houston), p. 152–174.
- Canals, M.; Catafau, E.; and Serra-Raventós, J. 1982. Toponímia de la mar catalano-balear (amb un glossary de termes genètics). *Boll. Soc. Hist. Nat. Balears* 26: 169–194.
- Canals, M.; Lastras, G.; Urgeles, R.; Casamor, J. L.; Mienert, J.; Cattaneo, A.; De Batist, M.; et al. 2004. Slope failure dynamics and impacts from seafloor and shallow sub-seafloor geophysical data: case studies from the COSTA project. *Mar. Geol.* 213:9–72, doi:10.1016/j.margeo.2004.10.001.
- Casas, D.; Ercilla, G.; Baraza, J.; Alonso, B.; and Maldonado, A. 2003. Recent mass-movement processes on the Ebro continental slope (NW Mediterranean). *Mar. Petrol. Geol.* 20:445–457, doi:10.1016/S0264-8172(03)00078-3.
- Dan, G.; Sultan, N.; and Savoye, B. 2007. The 1979 Nice harbour catastrophe revisited: trigger mechanism inferred from geotechnical measurements and numerical modelling. *Mar. Geol.* 245:40–64, doi:10.1016/j.margeo.2007.06.011.
- Dawson, A. G.; Long, D.; and Smith, D. E. 1988. The Storegga Slides: evidence from eastern Scotland for a possible tsunami. *Mar. Geol.* 82:271–276, doi:10.1016/0025-3227(88)90146-6.
- El-Robrini, M.; Genesseeux, M.; and Mauffret, A. 1985. Consequences of the El-Asnam earthquakes: turbidity currents and slumps on the Algerian margin (western Mediterranean). *Geo-Mar. Lett.* 5:171–176, doi:10.1007/BF02281635.
- Farran, M., and Maldonado, A. 1990. The Ebro continental shelf: Quaternary seismic stratigraphy and growth patterns. *Mar. Geol.* 95:289–312, doi:10.1016/0025-3227(90)90121-Y.
- Fine, I. V.; Rabinovich, A. B.; Bornhold, B. D.; Thomson, R. E.; and Kulikov, E. A. 2005. The Grand Banks landslide-generated tsunami of November 18, 1929: preliminary analysis and numerical modeling. *Mar. Geol.* 215:45–57, doi:10.1016/j.margeo.2004.11.007.
- Geist, E. L.; Lynett, P. J.; and Cahytor, J. D. 2008. Hydrodynamic modeling of tsunamis from the Currituck Landslide. *Mar. Geol.* 264:41–52, doi:10.1016/j.margeo.2008.09.005.
- Genesseeux, M.; Mauffret, A.; and Pautot, G. 1980. Les glissements sous-marins de la pente continentale niçoise et la rupture des câbles en mer Ligure (Méditerranée occidentale). *C. R. Acad. Sci. Paris* 290:959–962.
- Hamdache, M.; Peláez, J. A.; and Yelles-Chauche, A. K. 2004. The Algiers, Algeria earthquake (M_w 6.8) of 21 May 2003: preliminary report. *Seismol. Res. Lett.* 3: 360–367, doi:10.1785/gssrl.75.3.360.
- Harbitz, C. B. 1992. Model simulations of tsunamis generated by the Storegga Slides. *Mar. Geol.* 105:1–21, doi:10.1016/0025-3227(92)90178-K.
- Harbitz, C. B.; Løvholt, F.; Pedersen, G.; and Masson, D. G. 2006. Mechanisms of tsunami generation by submarine landslides: a short review. *Norw. J. Geol.* 86: 255–264.
- Hébert, H., and Alasset, P. J. 2003. The tsunami triggered by the 21 May 2003 Algiers earthquake. *CSEM/EMSC Newsl.* 20:10–12.
- Heinrich, P.; Piatanesi, A.; Okal, E. A.; and Hébert, H., 2000. Near-field modeling of the July 17, 1998, tsunami in Papua New Guinea. *Geophys. Res. Lett.* 27: 3037–3040, doi:10.1029/2000GL011497.
- Imamura, F., and Hashi, K. 2002. Re-examination of the source mechanism of the 1998 Papua New Guinea earthquake and tsunami. *Pure Appl. Geophys.* 160: 2071–2086, doi:10.1007/s00024-003-2420-2.
- Ivetskaya, T.; Shevchenko, G.; and Korolyov, P. 2010. Spectral analysis of Chilean tsunami (February 27, 2010) records on the Pacific coast of Russia. *Geophys. Res. Abstr.* 12:EGU2010-15697.
- Kulikov, E. A.; Rabinovich, A. B.; Thomson, R. E.; and Bornhold, B. D. 1996. The landslide tsunami of November 3, 1994, Skagway Harbor, Alaska. *J. Geophys. Res.* 101:6609–6615, doi:10.1029/95JC03562.
- Lambeck, K.; Antonioli, F.; Anzidei, M.; Ferranti, L.; Leoni, G.; Scicchitano, G.; and Silenzi, S. 2011. Sea level change along the Italian coast during the Holocene and projections for the future. *Quat. Int.*, doi:10.1016/j.quaint.2010.04.026.
- Lambeck, K., and Bard, E. 2000. Sea-level change along the French Mediterranean coast for the past 30,000 years. *Earth Planet. Sci. Lett.* 175:203–222.
- Lastras, G.; Canals, M.; Amblas, D.; Frigola, J.; Urgeles, R.; Calafat, A. M.; and Acosta, J. 2007. Slope instability along the northeastern Iberian and Balearic continental margins. *Geol. Acta* 5:35–47.
- Lastras, G.; Canals, M.; Amblas, D.; Lavoie, C.; Church, I.; De Mol, B.; et al. 2011. Understanding sediment dynamics of two large submarine valleys from seafloor data: Blanes and La Fonera canyons, northwestern Mediterranean Sea. *Mar. Geol.* 280:20–39, doi:10.1016/j.margeo.2010.11.005.
- Lastras, G.; Canals, M.; Hughes-Clarke, J. E.; Moreno, A.; De Batist, M.; Masson, D. G.; and Cochonat, P. 2002. Seafloor imagery from the BIG'95 debris flow, western Mediterranean. *Geology* 30:871–874, doi:10.1130/0091-7613(2002)030<0871:SIFTBD>2.0.CO;2.
- Lastras, G.; Canals, M.; Urgeles, R.; De Batist, M.; Calafat, A. M.; and Casamor, J. L. 2004a. Characterization of the recent BIG'95 debris flow deposit on the Ebro margin, western Mediterranean Sea, after a variety of seismic reflection data. *Mar. Geol.* 213:235–255, doi:10.1016/j.margeo.2004.10.008.
- Lastras, G.; Canals, M.; Urgeles, R.; Hughes-Clarke, J. E.; and Acosta, J. 2004b. Shallow slides and pockmark

- swarms in the Eivissa Channel, western Mediterranean Sea. *Sedimentology* 51:837–850, doi:10.1111/j.1365-3091.2004.00654.x.
- Lastras, G.; De Blasio, F. V.; Canals, M.; and Elverhøi, A. 2005. Conceptual and numerical modeling of the BIG'95 debris flow, western Mediterranean Sea. *J. Sediment. Res.* 75:784–797, doi:10.2110/jsr.2005.063.
- Lee, H. J.; Locat, J.; Desgagnés, P.; Parsons, J. F.; McAdoo, B. G.; Orange, D. L.; Puig, P.; Wong, F. L.; Dartnell, P.; and Boulanger, E. 2007. Submarine mass movements on continental margins. *In* Nittrouer, C. A.; Austin, J. A.; Field, M. E.; Kravitz, J. H.; Syvitski, J. P. M.; and Wiberg, P. L., eds. *Continental margin sedimentation: from sediment transport to sequence stratigraphy*. Oxford, Wiley-Blackwell, Intl. Assoc. Sedimentol. Spec. Publ. 37:213–274.
- Liu, P. L. F.; Woo, S. B.; and Cho Y. S. 1998. Computer programs for tsunami propagation and inundation. Ithaca, NY, School of Civil and Environmental Engineering, Cornell University, 111 p.
- López-Venegas, A. M.; ten Brink, U. S.; and Geist, E. L. 2008. Submarine landslide as the source for the October 11, 1918, Mona Passage tsunami: observations and modeling. *Mar. Geol.* 254:35–46, doi:10.1016/j.margeo.2008.05.001.
- Maillard, A., and Mauffret, A. 1993. Structure et volcanisme de la fosse de Valence (Méditerranée nord-occidentale). *Bull. Soc. Geol. Fr.* 164:365–383.
- Marcos, M.; Monserrat, S.; Medina, R.; Orfila, A.; and Olabarrieta, M. 2009. External forcing of meteorological tsunamis at the coast of the Balearic Islands. *Phys. Chem. Earth* 34:938–947.
- Masson, D. G.; Harbitz, C. B.; Wynn, R. B.; Pedersen, G.; and Løvholt F. 2006. Submarine landslides: processes, triggers and hazard prediction. *Philos. Trans. R. Soc.* 364:2009–2039, doi:10.1098/rsta.2006.1810.
- Mauffret, A. 2007. The northwestern (Maghreb) boundary of the Nubia (Africa) Plate. *Tectonophysics* 429: 21–44, doi:10.1016/j.tecto.2006.09.007.
- McSaveney, M. J.; Goff, J. R.; Darby, D. J.; Goldsmith, P.; Barnett, A.; Elliott, S.; and Nongkas, M. 2000. The 17 July 1998 tsunami, Papua New Guinea: evidence and initial interpretation. *Mar. Geol.* 170:81–92, doi: 10.1016/S0025-3227(00)00067-0.
- Mohrig, D.; Whipple, K. X.; Hondzo, M.; Ellis, C.; and Parker, G. 1998. Hydroplaning of subaqueous debris flows. *Geol. Soc. Am. Bull.* 110:387–394, doi:10.1130/0016-7606(1998)110<0387:HOSDF>2.3.CO;2.
- Monserrat, S.; Ibbetson, A.; and Thorpe, A. J. 1991. Atmospheric gravity waves and the Rissaga phenomenon. *Q. J. R. Meteorol. Soc.* 117:553–570, doi:10.1002/qj.49711749907.
- Muñoz, A.; Lastras, G.; Ballesteros, M.; Canals, M.; Acosta, J.; and Uchupi, E. 2005. Sea floor morphology of the Ebro shelf in the region of the Columbretes Islands, western Mediterranean. *Geomorphology* 72: 1–18, doi:10.1016/j.geomorph.2005.04.012.
- Nelson, C. H., and Maldonado, A. 1988. Factors controlling depositional patterns of Ebro turbidite systems, Mediterranean Sea. *Am. Assoc. Petrol. Geol. Bull.* 72:698–716.
- . 1990. Factors controlling late Cenozoic continental margin growth from the Ebro Delta to the western Mediterranean deep sea. *Mar. Geol.* 95:419–440, doi:10.1016/0025-3227(90)90127-6.
- Okal, E. A.; Synolakis, C. E.; Uslu, B.; Kalligeris, N.; and Voukouvalas, E. 2009. The 1956 earthquake and tsunami in Amorgos, Greece. *Geophys. J. Int.* 178:1533–1554, doi:10.1111/j.1365-246X.2009.04237.x.
- Otero, L. 2008. Metodología para evaluar la peligrosidad debido a tsunamis en costas españolas. PhD thesis, Universidad de Cantabria, Spain, 239 p.
- Papadopoulos, G. A.; Daskalaki, E.; Fokaefs, A.; and Giraleas, N. 2007. Tsunami hazards in the eastern Mediterranean: strong earthquakes and tsunamis in the East Hellenic Arc and Trench system. *Nat. Hazards Earth Syst. Sci.* 7:57–64.
- Papadopoulos, G. A., and Kortekaas, S. 2003. Characteristics of landslide generated tsunamis from observational data. *In* Locat, J., and Miernert, J. eds. *Submarine mass movements and their consequences*. Advances in natural and technological hazards research. Dordrecht, Kluwer Academic, p. 367–374.
- Pelinovsky, E., and Poplavsky, A. 1996. Simplified model of tsunami generation by submarine landslides. *Phys. Chem. Earth* 21:13–17, doi:10.1016/S0079-1946(97)00003-7.
- Pelinovsky, E.; Sladkevich, M.; Chubarov, L.; Didenkulovala, I.; Kit, E.; Shokin, Yu.; Beisel, S.; and Levin, A. 2009. The 1956 Greek tsunami recorded at Yafo (Israel) and its numerical modeling. *Geophys. Res. Abstr.* 11:EGU2009-131.
- Perissoratis, C., and Papadopoulos, G. 1999. Sediment instability and slumping in the southern Aegean Sea and the case history of the 1956 tsunami. *Mar. Geol.* 161:287–305.
- Rabinovich, A. B.; Thomson, R. E.; Kulikov, E. A.; Bornhold, B. D.; and Fine, I. V. 1999. The landslide-generated tsunami of November 3, 1994, in Skagway Harbor, Alaska: a case study. *Geophys. Res. Lett.* 26: 3009–3012, doi:10.1029/1999GL002334.
- Rahiman, T. I. H.; Pettinga, J. R.; and Watts, P. 2007. The source mechanism and numerical modelling of the 1953 Suva tsunami, Fiji. *Mar. Geol.* 237:55–70.
- Roca, E.; Sans, M.; Cabrera, L.; and Marzo, M. 1999. Oligocene to Middle Miocene evolution of the central Catalan margin (northwestern Mediterranean). *Tectonophysics* 315:209–233, doi:10.1016/S0040-1951(99)00289-9.
- Rzadkiewicz, S. A.; Mariotti, C.; and Heinrich, P. 1996. Modelling of submarine landslides and generated water waves. *Phys. Chem. Earth* 21:7–12, doi:10.1016/S0079-1946(97)00002-5.
- Shanmugam, G. 2000. 50 years of the turbidite paradigm (1950s–1990s): deep-water processes and facies models—a critical perspective. *Mar. Petrol. Geol.* 17:285–342, doi:10.1016/S0264-8172(99)00011-2.
- Skvortsov, A. 2002. Numerical simulation of landslide-generated tsunamis with application to the 1975 fail-

- ure in Kitimat Arm, British Columbia, Canada. PhD thesis, School of Earth and Ocean Sciences, University of Victoria, British Columbia.
- Soloviev, S. L.; Solovieva, O. N.; Go, C. N.; Kim, K. S.; and Shchetnikov, N. A. 2000. Tsunamis in the Mediterranean Sea 2000 B.C.–2000 A.D. *Advances in natural and technological hazards research*. Dordrecht, Kluwer Academic, 243 p.
- Sultan, N.; Cochonat, P.; Canals, M.; Cattaneo, A.; Denielou, B.; Haflidason, H.; Laberg, J. S.; et al. 2004. Triggering mechanisms of slope instability processes and sediment failures on continental margins: a geotechnical approach. *Mar. Geol.* 213:291–321, doi:10.1016/j.margeo.2004.10.011.
- Swafford, L., and Stein, S. 2007. Limitations of the short earthquake record for seismicity and seismic hazard studies. *Geol. Soc. Am. Spec. Pap.* 425:49–58.
- Tappin, D. R.; Matsumoto, T.; Watts, P.; Satake, K.; McMurtry, G. M.; Matsuyama, M.; Lafort, Y.; et al. 1999. Sediment slump likely caused 1998 Papua New Guinea tsunami. *EOS: Trans. Am. Geophys. Union* 80: 329, 334, 340, doi:10.1029/99EO00241.
- Tappin, D. R.; Watts, P.; and Grilli, S. T. 2008. The Papua New Guinea tsunami of 17 July 1998: anatomy of a catastrophic event. *Nat. Hazards Earth Syst.* 8:243–266, doi:10.5194/nhess-8-243-2008.
- ten Brink, U. S.; Lee, H. J.; Geist, E. L.; and Twichell, D. 2009. Assessment of tsunami hazard to the U.S. East Coast using relationships between submarine landslides and earthquakes. *Mar. Geol.* 264:65–73.
- TRANSFER 2009. Tsunami scenarios for the Balearic Islands with focus on Palma de Mallorca and flooding maps of Palma de Mallorca. Deliverable D8.3 of project Tsunami Risk and Strategies for the European Region (TRANSFER), 6th European Framework Program.
- Trifunac, M. D., and Todorovska, M. I. 2002. A note on differences in tsunami source parameters for submarine slides and earthquakes. *Soil Dynam. Earthq. Eng.* 22:143–155, doi:10.1016/S0267-7261(01)00057-4.
- Urgeles, R.; Leynaud, D.; Lastras, G.; Canals, M.; and Mienert, J. 2006. Back-analysis and failure mechanisms of a large submarine slide on the Ebro slope, NW Mediterranean. *Mar. Geol.* 226:185–206, doi:10.1016/j.margeo.2005.10.004.
- Wang, X. 2006. COMCOT user manual. Version 1.6. Technical report. Ithaca, NY, School of Civil and Environmental Engineering, Cornell University, 23 p.
- Wang, X., and Liu P. L. F. 2005. A numerical investigation of the Boumerdes-Zemmouri (Algeria) earthquake and tsunami. *Comput. Model. Eng. Sci.* 10:171–183.
- Watts, P.; Grilli, S. T.; Kirby, J. T.; Fryer, G. J.; and Tappin, D. R. 2003. Landslide tsunami case studies using a Boussinesq model and a fully nonlinear tsunami generation model. *Nat. Hazards Earth Syst.* 3:391–402.
- Watts, P.; Grilli, S. T.; Tappin, D. R.; and Fryer, G. J. 2005. Tsunami generation by submarine mass failure. II: predictive equations and case studies. *J. Waterw. Port Coast. Ocean Eng.* 131:298–310, doi:10.1061/(ASCE)0733-950X(2005)131:6(298).
- Whitmore, P.; ten Brink, U.; Caropolo, M.; Huerfano-Moreno, V.; Knight, W.; Sammler, W.; and Sandrik, A. 2009. NOAA/West Coast and Alaska Tsunami Warning Center Atlantic Ocean response criteria. *Sci. Tsunami Hazards* 28:86–107.